Recent Advances and Applications of "Successive Self-Nucleation and Annealing" (*SSA*) High Speed Thermal Fractionation

Alejandro J. Müller, Arnaldo T. Lorenzo, María L. Arnal*

Summary: The Successive Self-nucleation and Annealing (*SSA*) thermal fractionation technique is briefly reviewed to highlight recent advances such as the use of high speed DSC concepts to perform faster fractionation. Additionally, recent applications of *SSA* to characterize confined semi-crystalline model polyethylenes in block copolymer nanophases and *in situ* prepared nanocomposites with carbon nanotubes are also reviewed. A novel result presented here deals with the use of a macromolecular plasticizer to improve the quality of *SSA* thermal fractionation.

Keywords: block copolymers; high speed thermal fractionation; nanocomposites; SSA

Introduction

The Successive Self-nucleation and Annealing (*SSA*) thermal fractionation technique offers a practical way to evaluate chain heretogeneities in semicrystalline thermoplastic materials by employing a carefully designed thermal protocol easy to run in a Differential Scanning Calorimeter (*DSC*). The *SSA* technique is particularly useful to study the degree and distribution of short chain branches produced by the copolymerization of ethylene with α-olefins, however, other materials (i.e. copolymers and polyblends) have also been recently examined by the technique.[1–6] *SSA* thermal fractionation provides an alternative to experimentally more time consuming (such as Step Crystallization, SC) or complicated fractionation techniques, (such as Temperature Rising Elution Fractionation, (TREF) and Crystallization Analysis Fractionation (Crystaf)) that involve preparative or analytical fractionation in solution.[1]

The self-nucleation and annealing (*SSA*) technique was designed by Müller et al.[6] and consists on the sequential application of self-nucleation and annealing steps to a polymer sample.[1,7–11] After thermal conditioning, a final *DSC* heating run reveals the distribution of melting temperatures induced by the *SSA* thermal treatment as a result of the heterogeneous nature of the chain structure of the polymer under analysis. *SSA* can be performed at substantially shorter times (specially if High Speed *SSA* is employed) than *SC* and with better resolution.[1] The use of high speed calorimetry concepts[1,2,12] (high rates can be used as long as the sample mass is reduced accordingly) on the thermal fractionation given by *SSA* can yield qualitative results in record times.

A brief introduction to High Speed *SSA* thermal fractionation as well as the most recent applications of this technique for the thermal fractionation of semicrystalline block copolymers and polyethylene nanocomposites will be presented in this mini-review.

Experimental Part

Materials

A model polyethylene (PE^{25}) was obtained by the complete hydrogenation of an anionically synthetized high 1,4 polybutadiene (PB),[3] with an average number

Grupo de Polímeros USB, Departamento de Ciencia de los Materiales, Universidad Simón Bolívar. Apartado 89000, Caracas 1080-A, Venezuela
E-mail: amuller@usb.ve

molecular weight of 25 kg/mol, a polydispersity of 1.01 and 11 wt % 1,2 units content. Two sets of polyethylene (PE) containing diblock copolymers: with polystyrene (PS) and poly(ethylene-*alt*-propylene) (PEP) as second blocks (see Table 1 for molecular data).[3,4]

The notation used for the copolymers is the following: $A_xB_y^m$, where the subscript numbers denote the mass fraction in weight percent and the superscripts give the number-averaged molecular weight $\overline{M}_n$ in kg/mol of the entire block copolymer.

Finally, high-density polyethylene/carbon nanotubes (HDPE/CNT) nanocomposites prepared by *in situ* polymerization techniques were evaluated (see reference 5 for a detailed explanation of the preparation method). Table 2 shows the composition and identification of all the nanocomposites studied. For comparison purposes a neat HDPE homopolymer was synthesized using similar conditions to those employed for the nanocomposites.[5,6] Three types of CNT were used: single wall (SWNT), double wall (DWNT) and multi wall (MWNT). The following nomenclature is used to indicate the composition of the samples: $PE_xS_yAl_z$ where the subscripts indicate the % weight contents of each component present in the formulation (HDPE, CNT and Al_2O_3 respectively), the letter S is used to denote SWNT, other samples with letters D or M indicate DWNT or MWNT.

Differential Scanning Calorimetry (DSC)

Differential scanning calorimetry (DSC) was performed with a Perkin Elmer Pyris 1 instrument calibrated with indium and tin under an ultra high purity nitrogen atmosphere. Sample weights varied between 1 and 10 mg, depending on the scanning rate employed, and they were encapsulated in aluminum pans and sealed. The crystalline thermal history was erased by heating the samples at least 30 °C above their respective peak melting temperature for 3 min. Scanning rates (in °C/min) are indicated within the figures or figure captions.

Results and Discussion

Successive Self-nucleation and Annealing (SSA) Thermal Fractionation Method

In the *SSA* protocol[1,7–8] the following steps are performed (see Figure 1 for a graphic explanation): **(a)** The sample is held in the melt (circa 30 °C above its respective peak melting temperature) for 3 min to erase thermal history. **(b)** The sample is cooled, at a constant rate, to the lower temperature limit in order to allow the crystallization of

Table 1.
Characteristics of the diblock copolymer employed.[3,4]

Copolymers	Wt PE[a]	ϕPE[b]	$\overline{M_n}$ (kg/mol)	PE	PEP	PEP	Polydisp.
			PE block[c]	% 1,2 Units[d]	% 1,4 Units[d]	% 1,2&3,4 Units[d]	D[c]
PE^{25}	–	–	25	11.0	–	–	1.01
$E_{53}S_{47}^{51}$	0.53	0.57	27	11.3	–	–	1.04
$E_{26}S_{74}^{105}$	0.26	0.29	27	11.3	–	–	1.05
$E_{11}S_{89}^{244}$	0.11	0.13	27	11.3	–	–	1.02
$E_{54}EP_{46}^{53}$	0.54	0.52	29	11.2	88.7	11.3	1.02
$E_{29}EP_{71}^{99}$	0.29	0.28	29	11.9	86.4	13.6	1.02
$E_{12}EP_{88}^{238}$	0.12	0.11	28	11.2	88.8	11.2	1.03

[a]Weight fraction of the PE block.
[b]PE block volumetric fraction determined assuming additive volumes. Densities at room temperature of the PE semicrystalline block were employed using the corresponding crystallinity degrees calculated by DSC, and crystalline and amorphous values taken from the literature ($\rho_{PS} = 1.05$ g/cm^3; $\rho_{am\text{-}PE} = 0.887$ g/cm^3; $\rho_{cr\text{-}PE} = 0.999$ g/cm^3; $\rho_{PEP} = 0.854$ g/cm^3).
[c]Determined by SEC experiments.
[d]Determined by ^{1}H NMR experiments.

Table 2.
HDPE/CNT nanocomposites evaluated: HDPE/SWNT ($PE_xS_yA_z$), HDPE/DWNT ($PE_xD_yA_z$), HDPE/MWNT ($PE_xM_yA_z$).[5,6]

Name	Type	CNT content[a] (%)	HDPE content[a] (%)	Al_2O_3 content[a] (%)
HDPE	–	–	92.4	7.60
$PE_{87}S_8A_5$	SWNT	7.57	87.07	5.36
$PE_{56}S_{20}A_{24}$	SWNT	20.05	56.08	23.87
$PE_{33}S_{36}A_{31}$	SWNT	33.21	36.21	30.58
$PE_{82}D_8A_{10}$	DWNT	7.6	82.20	10.17
$PE_{60}D_{17}A_{23}$	DWNT	17.35	60.16	22.49
$PE_{44}D_{26}A_{30}$	DWNT	26.19	43.45	30.36
$PE_{83}M_6A_{11}$	MWNT	5.91	82.55	11.53
$PE_{68}M_{11}A_{21}$	MWNT	11.15	68.21	20.64
$PE_{41}M_{26}A_{33}$	MWNT	26.41	41.06	32.53

[a]The compositions were determined by Thermogravimetry analysis (TGA). Table 2 show that the CNT are present in the samples in three different contents: low (5–8%), medium (11–20%) and high (26–33%). The diameters of the CNT employed were determined by TEM and the results yield: 2, 4 and 5–27 nm for SWNT, DWNT and MWNT respectively.

the material. The peak crystallization temperature recorded during this cooling scan will be referred to as the ''standard'' crystallization temperature (or standard T_c). **(c)** Self-nucleation step (or self-nucleation and annealing).[1,13] The sample is heated at a constant rate (the same rate employed in step (b)) from the lower temperature limit to a selected self-seeding temperature (that we shall term T_s). (d) The sample is held at this T_s for 5 min. This isothermal treatment at T_s results in partial melting and, depending on T_s, in the annealing of unmelted crystals, while some of the melted species may isothermally crystallize (after being self-nucleated by the unmelted crystals). **(e)** Cooling from T_s: The sample is cooled at a constant rate from T_s to the lower temperature limit, the fraction of the polymer that was melted at T_s will crystallize during cooling, depending on the T_s applied in step (c). If the sample is in *Domain I* (or complete melting *Domain*) it will crystallize at the standard T_c, if it is in *Domain II* (or exclusive self-nucleation *Domain*) it will crystallize at a higher temperature since it will be self-nucleated, and finally, if it is in *Domain III* (or self-nucleation and annealing *Domain*) it will immediately crystallize during cooling (just below T_s).[1,13] **(f)** Steps ''c'', ''d'' and ''e'' were repeated at progressively lower T_s. The number of repetitions (cycles) can be chosen to cover the entire melting range of the sample with a ''standard'' thermal history or a shorter range. For example, in the case of the model PE[25] only 7 cycles were applied (from 102 °C to 72 °C). When heating to a new T_s or fractionation step: The sample is heated once again at the same constant rate previously selected, but this time to a new T_s which is usually 5 °C lower (a different fractionation window may be selected depending on the application, see Ref. 1 for details) than the previous T_s. The sample is held at this new T_s for 5 min. This treatment causes the unmolten crystals at this T_s to anneal and therefore the lamellae to thicken, some of the melted species may isothermally crystallize (after being self-nucleated by the unmelted crystals),

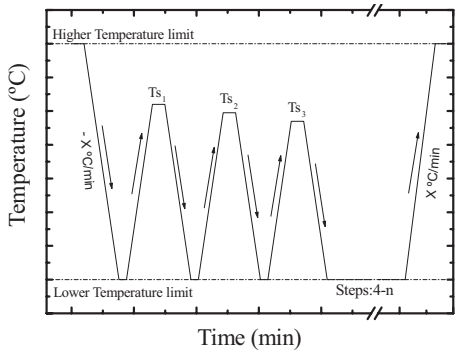

Figure 1.
SSA thermal protocol model. Cooling and Heating scans are performed at X °C/min scanning rate.

while the rest of the molten crystallizable chain segments will only crystallize during the subsequent cooling from T_s. This step is crucial for the fractionation process, since it defines the fractionation window or temperature interval selected for the fractionation, i.e., in this case a $\Delta T = 5\,^{\circ}C$ and a fractionation time of only 5 min. The effects of changing ΔT, time and the initial T_s have been reviewed in the literature[1]. **(g)** Final melting: The sample was heated at the chosen constant rate up to the melt state.

In a previous work from our group,[1] *SSA* thermal protocol has been performed employing a constant sample mass (approximately 10 mg) and various heating rates (5, 10 and 20 °C/min). Under these conditions, the best time-resolution compromise was obtained by employing 10 °C/min scanning rates. Later on we incremented the scanning rates up to 50 °C/min following Pijpers et al.[11] recommendations that an increment in heating rates needed to be compensated by reducing sample mass. Experiments have been carried out with the model PE^{25} and, as a result, Figure 2 demonstrates that *SSA* can be performed employing rates as high as 50 °C/min using a conventional *DSC* equipped with an intra cooler device. Figure 2 shows how the resolution at high (50 °C/min) and low scanning rates (5 °C/min) is almost identical, when the mass has been conveniently reduced to avoid any superheating effects. A slight shift (less than 1 °C) of the melting point of the fraction to higher temperatures is barely noticeable.[1,2,12] The *SSA* fractionated PE^{25} final *DSC* heating scan shows the effects of the accumulation of 7 self-nucleation and annealing steps using T_s ranging from 102 to 72 °C, every 5 °C. Since 102 °C is the ideal self-nucleation temperature for this polymer,[1,2] the thermal treatment at this T_s does not cause any annealing. Therefore, only 6 steps were able to produce annealing. Figure 2 shows the 6 sharp melting peaks of PE^{25} obtained after *SSA* plus an additional broad melting peak (at around 65 °C) corresponding to crystals formed during cooling from the lowest T_s employed.

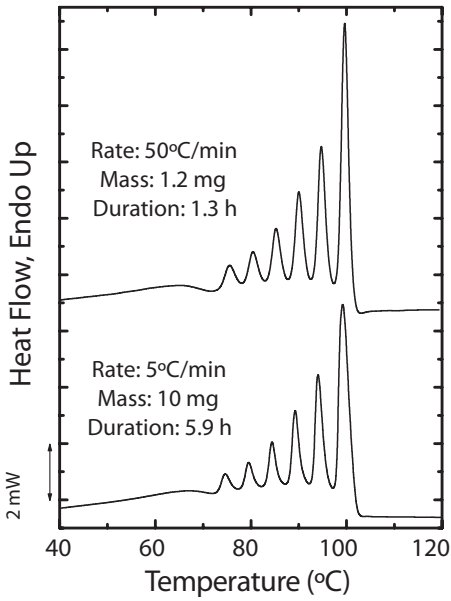

Figure 2.
Final heating scans for the PE^{25} after applying the *SSA* thermal treatment at different scanning rates. At 50 °C/min the quality of the fractionation is very good for PE^{25} and the fractionation time has been reduced from 5.9 to 1.3 hours (70% time saving gain).

It is evident that applying the *SSA* fractionation technique with higher heating and cooling rates (i.e., at least 50 °C/min) the time reduction is even greater, since the isothermal steps in *SSA* are only 5 min long. Even higher heating and cooling rates are in principle possible,[12] however, special equipment and/or cooling devices may be needed (some new commercial DSC equipments already incorporate high speed capabilities).

Thermal Fractionation of PE Nanocomposites with Carbon Nanotubes (CNT)

In Figure 3 the final heating scan after *SSA* thermal fractionation for neat HDPE is shown. This polymer exhibits only two dominating endotherms whose melting peaks are very close to each other (131.6 and 129.6 °C) and are the product of the thermal fractionation achieved during the first three fractionations steps applied (i.e., 133, 128 and 123 °C, where 133 °C only

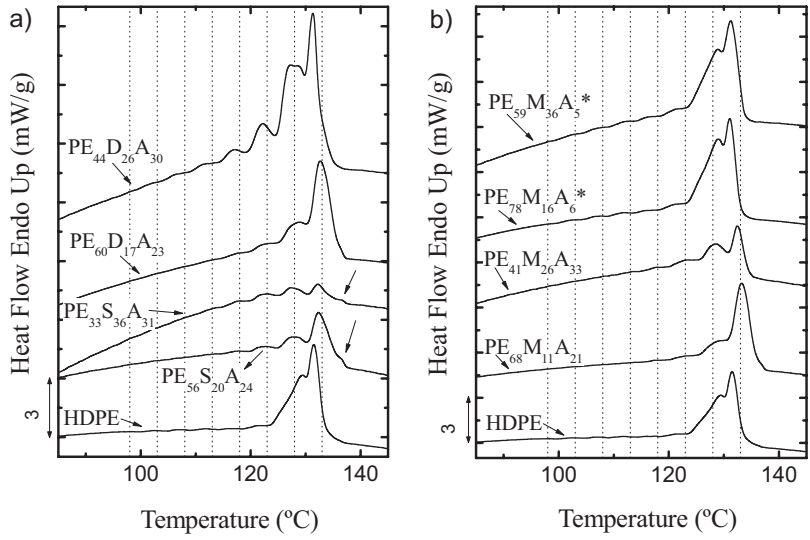

Figure 3.
DSC heating scans at 10 °C/min after *SSA* thermal treatment fractionation for: (a) PExSyAz and PExDyAz, (b) PExMyAz and PExMyAz*. Also, a PEAD *SSA* curve is presented for comparison.

causes self-nucleation in HDPE, while the other two produce self-nucleation plus annealing). The rest of the thermal fractions produced are five small endotherms clearly defined by the other 5 T_s temperatures applied, but they are less important in magnitude. The thermal fractionation of analogous HDPE materials has already been reported in the literature with similar results.[1,14,15]

The results of applying the same *SSA* treatment (the same used for the HDPE) to the *in situ* nanocomposites containing different amounts of CNT are also presented in Figure 3. One of the most important differences observed is the appearance of a new high temperature fraction which is not present in the HDPE. This new fraction is consistent with reported higher melting points for the nanocomposites (especially at low CNT contents) as compared to HDPE as well as higher *Domain I* to *III* transition temperatures.[5,6] This change in the distribution of melting points in the *in situ* nanocomposites has occurred as compared to neat HDPE and the change is much more noticeable as the content of CNT increases. Figure 3 results indicate that in those *in situ* nanocomposites where the PE phase is 60% or lower in content, a change in the fractionation resolution has been achieved.

This *SSA* treatment was also applied to a physical blend of HDPE and MWNT of analogous compositions (we named these blends as PExMyAz*) to the *in situ* prepared nanocomposites. The results are also shown in Figure 3b. The behavior is totally different to that exhibited by the *in situ* nanocomposites. In this case, the shape of the multimodal endotherm is comparable within the experimental error to that observed for HDPE. In this case, the MWNT mechanically incorporated in HDPE in the melt do not promote the formation of more stable thicker lamellae that melt at higher temperatures. In this blend the dispersion obtained is not very good since the disaggregation characteristic of the *in situ* polymerization is not present. In conclusion, these results indicate that lamellar crystals formed during the *SSA* treatment (corresponding to the highest melting thermal fraction) in *in situ* polymerized samples with CNT formed thicker and more stable crystals than those produced under equivalent conditions in neat HDPE. The reason for this behavior is the

peculiar bottle brush morphology achieved during crystallization by chains that are nucleated on the surface of CNT.[5]

Confinement Effects on the Thermal Fractionation of PE-*b*-PS diblock Copolymers

Figure 4 shows a final heating *DSC* scan after *SSA* fractionation was performed to PE^{25} and to the PE-*b*-PS block copolymer samples. Since the copolymers were synthesized from precursors whose polybutadiene blocks were the same, the microstructure of the PE blocks and their molecular weights (along with their distributions) are kept constant. Therefore, any departure from the *SSA* behavior of the homo-PE^{25} can only be attributed to topological changes. The fractionated PE^{25} clearly shows a series of melting peaks that correspond to the melting of crystalline fractions of different mean lamellar thickness that formed and annealed at each T_s temperature employed. Figure 4 also contains final heating scans for four PE-*b*-PS diblock copolymers. Even in the $E_{79}S_{21}^{41}$ diblock copolymer, whose morphology is a PE matrix with glassy polystyrene cylinders (as demonstrated previously, ref. 3), the distribution of lamellar thickness obtained after *SSA* fractionation is different from that of PE^{25}. In Figure 4, the fraction named "1" (the one annealed at $T_s = 97\,^{\circ}C$) decreases in area as the PS content increases in the copolymer, until it totally disappears for the $E_{11}S_{89}^{244}$ copolymer (PE spheres in a PS matrix). This phenomenon can be observed in a similar way for the second and third fractions (annealed at 92 and 87 °C, respectively). In general, a decrease in the high temperature melting peak areas and an increase in the low temperature melting peak areas are observed as the composition (PS content) varies in the copolymer.

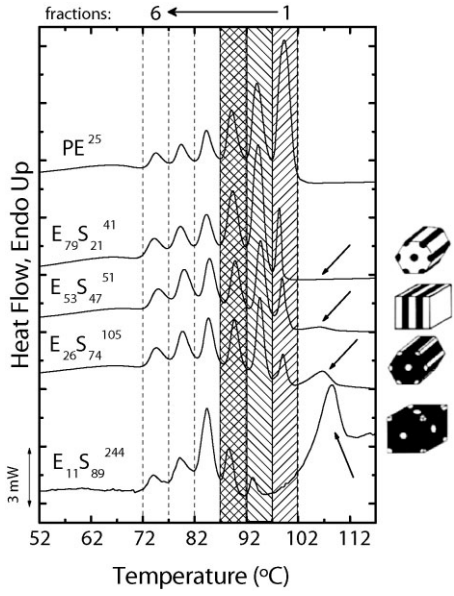

Figure 4.
DSC heating scans at 10 °C/min for PE^{25} and the PE-*b*-PS diblock copolymers after the *SSA* thermal treatment. The curves were normalized to the PE content within the block copolymer. The arrows indicate the glass transition for the PS component. The cartoons illustrate the morphology of the copolymer, black refers to PS microdomains and white to PE microdomains.

The *SSA* method allows the qualitative observation of the topological chain restrictions associated with the crystallization of the PE block as the morphology changes from a PE matrix ($E_{79}S_{21}^{41}$), to PE lamellae ($E_{53}S_{47}^{51}$), PE cylinders ($E_{26}S_{74}^{105}$) and finally to PE spheres ($E_{11}S_{89}^{244}$) within the diblock copolymers and in comparison to the PE^{25} homopolymer sample[3]. For instance, for the $E_{11}S_{89}^{244}$ the most abundant fraction of lamellae are the ones that were originated at a T_s of 82 °C (fraction number 4) while in the PE^{25} this fraction was only the fourth most important and much less abundant. Since no change in the distribution of *SCB* is present in the PE phase for all samples (due to the synthesis procedure and the %1,2 units), all changes in the distribution of melting points (or lamellar thickness) must be accounted for by morphological restrictions caused by the vitreous PS matrix on the PE domains.

As topological confinement increases, the higher melting temperature fractions progressively disappear as large crystals cannot be accommodated easily within the micro and nano phase segregated domains.

Diluent Effect of the PEP Block upon the PE Thermal Fractionation of PE-*b*-PEP Diblock Copolymers

Figure 5 shows the diluent effects of the PEP block upon the *SSA* thermal fractionation of the PE component as compared with the PE^{25} homopolymer. The shape and distribution of the melting peaks obtained after applying the *SSA* protocol is notably different in the PE-*b*-PEP diblock copolymers. It has been established how the presence of a diluent blended with the amorphous zones of a semicrystalline polymers trends to decrease the melting temperatures of the crystal families produced even though they may be similar to the ones observed in the neat polymer (diluent free).[16]

Even though the diluent is expected to cause a depression of the melting points of each fraction, one would anticipate that the distribution of melting points should not change significantly, since in this case there are no confinement effects present (except for the $E_{12}EP_{88}$ where the extreme dilution of the PE block has been demonstrated to cause hindrance to the crystallization process, see ref. 4). Nevertheless, there is an important change in the distribution of melting points, compare in Figure 5 the distribution of melting points for PE^{25} and for $E_{54}EP_{46}$ and $E_{29}EP_{71}$, since for the copolymers the highest melting fraction (or fraction 2) is less important than fraction 3. We therefore postulate that fraction 2 in the PE block of the copolymers is a new fraction, which, thanks to the plasticization effect provided by the macromolecular diluent PEP block, can be formed, while it is not present in PE^{25} fractionated under the same conditions. In order to prove this hypothesis we have represented some of the DSC traces of Figure 5 as a function of supercooling in Figure 6.

When the DSC traces are represented as a function of supercooling, we normalize

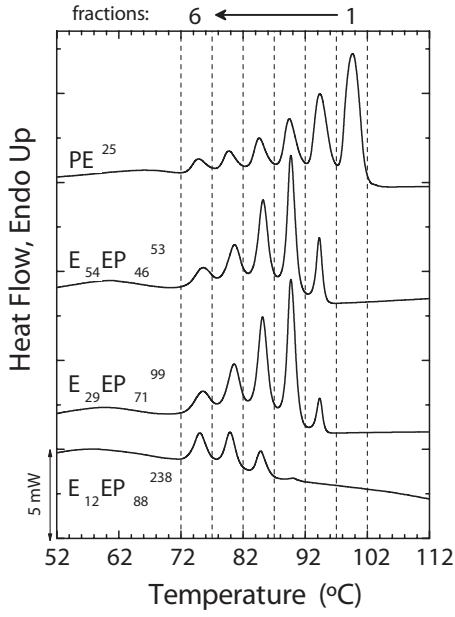

Figure 5.
DSC heating scans at 10 °C/min for PE^{25} and the PE-*b*-PEP diblock copolymers after the *SSA* thermal treatment. The curves were normalized in function to the PE content within the block copolymer.

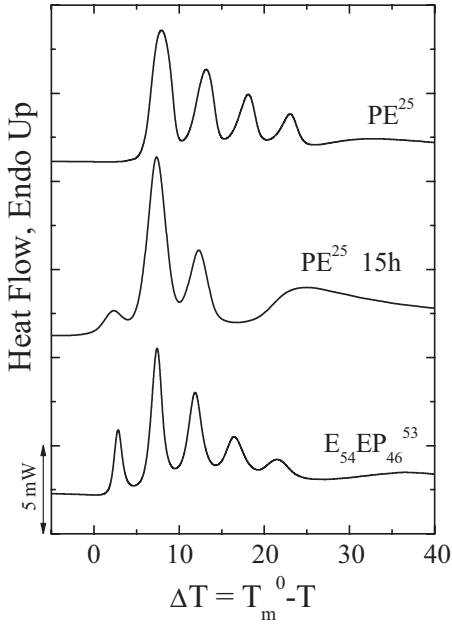

Figure 6.
DSC heating scans at 10 °C/min versus the degree of supercooling (ΔT) for PE^{25} and the $E_{54}EP_{46}^{53}$ diblock copolymer after the *SSA* thermal treatment (taken from Figure 5). A DSC heating scan for the PE^{25} after applying the *SSA* thermal protocol with holding times of 15 hours is also presented.

the data by the dilution effect, therefore, it can be clearly seen that in PE^{25} fractionated using the same experimental parameters as in $E_{54}EP_{45}$, the thermal fraction nearest to the thermodynamic equilibrium (the one with the smallest supercooling in $E_{54}EP_{45}$) is not present in PE^{25}. In order to generate this fraction in PE^{25}, we repeated the *SSA* fractionation procedure but employing holding times of 15h (a smaller number of fractionation steps were applied), the final heating scan is also represented in Figure 6 and a new small endotherm at very small supercoolings is generated. In other words, because of the absence of the plasticizing effect of the molecularly bonded PEP (in the copolymer), in the case of homo-PE, much longer times are needed to produce an equivalent fractionation. This is a novel concept that we are now investigating and which may lead to new ways to produce higher sensitivity thermal fractionation.

Conclusions

High speed DSC concepts can be used to accelerate substantially the time needed to produce thermal fractionation in ethylene/α-olefin copolymers or any other polymer whose linear crystallizing sequences are interrupted by chain defects (branches, stereo-irregularity, etc.). The *SSA* technique can be employed to reveal morphological and topological differences arising from different chain environments as in the two examples presented here dealing with PE/CNT nanocomposites and topological confinement within micro and nano domains of block copolymers. Finally, in the case of a miscible diblock copolymer, like PE-*b*-PEP, where the PEP can be consider a macromolecular solvent molecularly bonded to PE, the *SSA* fractionation can be improved by the excess molecular mobility of PE chains in such a way that fractions closer to thermodynamic equilibrium can be generated.

Acknowledgements: The authors acknowledge financial support from the Decanato de Investigación y Desarrollo of Simón Bolívar University through grant DID-GID-G02. We also thank V. Abetz, A. Boschetti de Fierro, Ph. Dubois, D. Bonduel, St. Bredeau, M. Trujillo and E. Laredo for their valuable cooperation.

[1] A. J. Müller, M. L. Arnal, *Prog. Polym. Sci.* **2005**, *30*, 559.
[2] A. T. Lorenzo, M. L. Arnal, A. J. Müller, A. Boschetti de Fierro, V. Abetz, *Macromol. Chem. Phys.* **2006**, *207*, 39.
[3] A. T. Lorenzo, M. L. Arnal, A. J. Müller, A. Boschetti-de-Fierro, V. Abetz, *Eur. Polym. J.* **2006**, *42*, 516.
[4] A. T. Lorenzo, M. L. Arnal, A. J. Müller, A. Boschetti-de-Fierro, V. Abetz, *Macromolecules* **2007**, *40*, 5023.
[5] M. Trujillo, M. L. Arnal, A. J. Müller, St. Bredeau, D. Bonduel, Ph. Dubois, I. W. Hamley, V. Castelleto, *Macromolecules* **2008**, *41*, 2087.
[6] M. Trujillo, M. L. Arnal, A. J. Müller, E. Laredo, St. Bredeau, D. Bonduel, Ph. Dubois, *Macromolecules* **2007**, *40*, 6268.
[7] A. J. Müller, Z. H. Hernández, M. L. Arnal, J. J. Sánchez, *Polym. Bull.* **1997**, *39*, 465.
[8] M. L. Arnal, V. Balsamo, G. Ronca, A. Sánchez, A. J. Müller, E. Cañizales, C. Urbina de Navarro, *J. Therm. Anal. Cal.* **2000**, *59*, 451.
[9] M. Zhang, D. T. Lynch, S. E. Wanke, *Polymer* **2001**, *42*, 3067.
[10] P. Starck, K. Rajanen, B. Löfgren, *Thermochim. Acta.* **2003**, *395*, 169.
[11] M. Zhang, S. Wanke, *Polym. Eng. Sci.* **2003**, *43*, 1878.
[12] T. F. J. Pijpers, V. B. F. Mathot, B. Goderis, R. L. Scherrenberg, E. W. van der Vegte, *Macromolecules* **2002**, *35*, 3601.
[13] B. Fillon, J. C. Wittman, B. Lotz, A. Thierry, *J. Polym. Sci. B.* **1993**, *31*, 1383.
[14] M. L. Arnal, E. Cañizales, A. J. Müller, *Polym. Eng. Sci.* **2002**, *42*, 2048.
[15] M. L. Arnal, J. J. Sánchez, A. J. Müller, *Polymer* **2001**, *42*, 6877.
[16] B. Hech, G. Strobl, M. Grasruck, *Eur. Phys. J. E.* **2003**, *22*, 117.

